17th World Conference on Earthquake Engineering, 17WCEE
Sendai, Japan - September 13th to 18th 2020

Cyclic Loading Test of Cruciform Frame Using High Strength Steel Box－Section Column to Beam Moment Connection with Exterior Diaphragm

R. Oba[(1)], H. Morioka[(2)], T. Kinoshita[(3)], Y. Koetaka[(4)], K. Suita[(5)] and Y. Murakami[(6)]

[(1)] *Staff, Construction Materials Engineering Dept., JFE Steel Corp., M. Eng., r-oba@jfe-steel.co.jp*
[(2)] *Researcher, Civil Engineering Dept., Steel Research Lab., JFE Steel Corp., M. Eng., hi-morioka@jfe-steel.co.jp*
[(3)] *Senior Researcher, Civil Engineering Dept., Steel Research Lab., JFE Steel Corp., Dr. Eng., to-kinoshita@jfe-steel.co.jp*
[(4)] *Assoc. Prof., Dept. of Architecture and Architectural Eng., Kyoto University, Dr. Eng., koetaka@archi.kyoto-u.ac.jp*
[(5)] *Prof., Dept. of Architecture and Architectural Eng., Kyoto University, Dr. Eng., suita@archi.kyoto-u.ac.jp*
[(6)] *Staff General Manager, Construction Materials Engineering Dept., JFE Steel Corp., M. Eng., yu-murakami@jfe-steel.co.jp*

Abstract

In recent years, high strength steels, whose tensile strength is more than 780MPa, have been developed in Japan and are used mainly for columns of high rise buildings. However, in case of high strength steels, not only securing strength and toughness of welding parts but also preventing cold crack need severer welding conditions, i.e. low heat input, preheat and afterheat, than in case of ordinary steels. In Japan, square hollow sections are most well used for columns, and stiffeners at the joint with the beam flange, i.e. diaphragms, are necessary to restrain local deformation of the joint. In this study, exterior-diaphragm type high strength 780MPa steel box-section column to beam moment connections are focused on, because this type of diaphragm has advantage to overcome the difficulties being faced during welding of high strength steels. To improve convenience of construction and transportation efficiency of columns preassembled with exterior diaphragms at fabrication factories, this study introduces square exterior diaphragms with the thick steel plates, whose depth is smaller than conventional exterior diaphragms.

In case of exterior diaphragms, local deformation of the joint, more specifically out-of-plane deformation of the column and in-plane deformation of the exterior diaphragm, occurs against the force transferred from the beam flange. Therefore, the methods to evaluate the elastic stiffness and the yield strength of beam-to-column connections in consideration of local deformation of the joints are essential for structural design. We have proposed evaluation methods of the elastic stiffness and the yield strength of beam flange joints theoretically with partial tensile models, and the validity of evaluation methods has been confirmed based on experiment or FEA in Ref.2 and 3. However, in Ref.2, concrete filled steel tube column (CFT column), which is generally adapted for columns of high rise buildings, to beam flange joints have not been studied, and evaluation methods of the elastic stiffness and the yield strength of beam-end connections including beam web joints have not been proposed. Consequently, it is needed to clarify elasto-plastic behaviors of beam-to-column connections, on which each of the hollow column and the CFT column is adopted.

First, outline of evaluation methods of the elastic stiffness and the yield strength are described based on Ref.2. FEA of box-section CFT column-to-beam flange connections with the exterior diaphragm is conducted to compare calculated values based on Ref.2 to numerical results. As a result, it is clarified that most calculated values of the elastic stiffness correspond numerical results with discrepancy of about 10 - 30 %. Furthermore, it is verified that the evaluation method of the yield strength proposed in Ref.2 is appropriate for predicting the elastic limit strength even in case of the CFT column.

Additionally, assuming the stress state and the deformation state of the beam-end connection for each of hollow columns and CFT columns, evaluation methods of the elastic stiffness and the yield strength of column to beam-end connections are proposed in this paper. In order to compare calculated values to experimental and numerical values, cyclic loading test and FEA of cruciform frames are conducted. As a results, it is verified that calculated values of the elastic stiffness and the yield strength of connections are able to evaluate most numerical results with discrepancy about 10 - 30 %. Further, in case of specimens designed with the yield strength of connections exceeding the bending moment acted at the beam-end under the plastic strength of the beam, it is confirmed that beam-end connections keep elastic until ultimate states of specimens, while plastic deformation of beams occurs dominantly, in experiment and FEA.

Keywords: High strength 780MPa class steel, Exterior diaphragm, CFT column, Loading test, Elastic stiffness

1. Introduction

In recent years, high strength steels, whose tensile strength is more than 780MPa, have been developed in Japan and are used mainly for columns of high rise buildings. In general, in case of 780MPa steel, severe construction management and advanced technique of welding, i.e. low heat input, preheat and afterheat, are required to not only secure the strength and the toughness of welding parts but also prevent cold crack, than in case of ordinary steels[1]. In particular, welding construction at beam to high strength steel column connections is very important.

In Japan, square hollow section columns are usually used in order to make bi-directional bending moments resisting frames. This type of closed cross section is necessary to stiffen sections by diaphragms at locations of beam flange joints to restrain local deformation. Through diaphragms and interior diaphragms shown in respectively Fig.1(a) and (b) are generally adapted at beam to column connnections of Japanese steel structures. In case of using the 780MPa steel for columns, at the through diaphragm type connection, columns and through diaphragms are connected by full penetration welding, and strengths of diaphragms and welding materials must be generally higher than that of columns. However, there is a possibility that the strength of welding parts is lower than that of 780MPa steels, depending on welding conditions. Thereby, severe welding conditions are needed to secure appropriate strength of welding parts, and it is difficult to adapt through diaphragms at beam to high strength 780MPa steel column connections in terms of welding workability. On the other hand, at the interior diaphragm type connection, electroslag welding is generally adapted. However, because electroslag welding needs extremely high heat input, securing the appropriate toughness of welding parts is difficult in case of high strength 780MPa steels. Therefore, in this study, we focus on the exterior diaphragm type connection shown in Fig.1(c). Because the diaphragm plate is attached only from outside of the column at the exterior diaphragm type connection, columns need not to be cut, and diaphragms and welding materials, whose strengths are equal to or more than that of beams, can be generally used. Furthermore, it is possible that CO_2 arc fillet welding is adapted. Therefore, this type of diaphragms has advantage to overcome difficulties being faced during welding of high strength 780MPa steels. To improve convenience of construction and transportation efficiency of columns preassembled with exterior diaphragms at fabrication factories, this study introduces square exterior diaphragms with thick steel plates shown in Fig.2(a), whose depth is smaller than conventional exterior diaphragms shown in Fig.2(b).

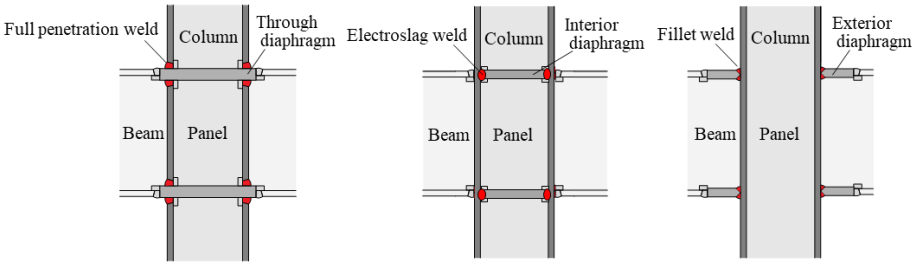

(a)Through diaphragm (b)Interior diaphragm (c)Exterior diaphragm

Fig.1 - Kinds of diaphragm type connections

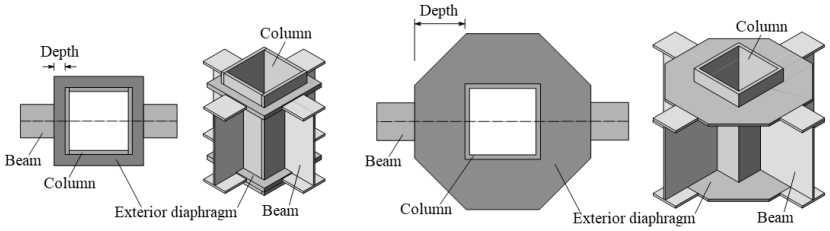

(a)Proposed type (b)Conventional type

Fig.2 - Exterior diaphragm

When the beam to column connection with exterior diaphragms is subjected to the bending moment *M*, out-of-plane deformation of column shown in Fig.3(a) and in-plane deformation of exterior diaphragm shown in Fig.3(b) generally occur, and there is possibility that the stiffness and the strength of exterior diaphragm

type connections are lower than those of through diaphragm type connections and interior diaphragm type connections. Accordingly, the appropriate methods to evaluate the elastic stiffness and the yield strength of beam to column connections are necessary to design connections. In Ref.2 and 3, we have proposed evaluation methods of the elastic stiffness and the yield strength of beam flange joints surrounded by the broken line in Fig.3(a) by loading tests and finite element analysis (FEA). However, Ref.2 has focused on only hollow box-section columns, and has not discussed concrete-filled tube columns (CFT columns), which is adapted in most high rise buildings. Therefore, in Chapter 2 (Section 2.1), evaluation methods of the elastic stiffness and the yield strength of beam flange joints proposed in Ref.2 are outlined, and in Chapter 3, the evaluation methods of Ref.2 are applied to CFT columns by FEA. In addition, Ref.2 has dealt only with beam flange joints, and has not yet proposed evaluation methods of the elastic stiffness and the yield strength of entire beam-end connections including beam web joints. In Chapter 2 (Section 2.2), evaluation methods of the elastic stiffness and the yield strength of beam-end connections are established for both hollow columns and CFT columns. Furthermore, in chapter 4, both elasto-plastic behaviors of beam-end connections and the validity of these evaluation methods is confirmed by loding tests and FEA.

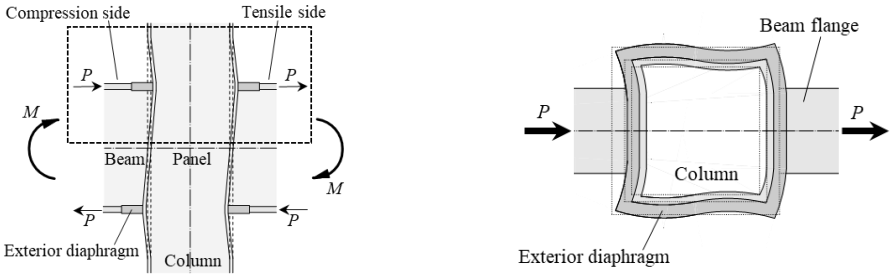

(a)Out-of-plane deformation of column (b)In-plane deformation of diaphragm

Fig.3 - Deformation of column and exterior diaphragm

2. Elastic Stiffness and Yield Strength of connection

2.1 Beam flange joint

In Ref.2, beam flange joints of hollow columns have been modeled as the exterior diaphragm model (Fig.4) and the column model (Fig.5) to calculate the elastic stiffness K and the yield strength P_y of beam flange joints.

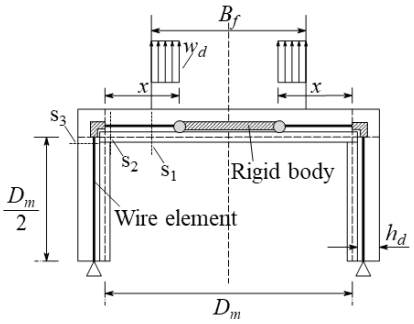

Fig.4 - Exterior diaphragm model[2]

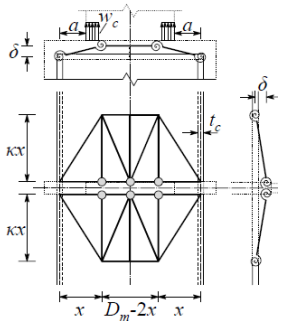

Fig.5 - Column model[2] (by RBSM)

The exterior diaphragm model is made of the exterior diaphragm and steel tube wall of column, whose length of the axial direction of the column is t_d (t_d is diaphragm thickness), and these sections are replaced with elasto-plastic wire elements having the rectangular cross section. Rigid bodies are located at shaded areas of corners and the center of the diaphragm. In addition, in Fig.4, pinned supports are provided at boundary positions between the tensile side and the compression side. The elastic stiffness K_d of the exterior diaphragm model can be obtained by considering the bending, shearing and axial deformation of wire elements. On the other hand, the column model shown in Fig.5 is applied to rigid-body spring model (which is called RBSM[4]) in the range of $2\kappa x$ in axial direction of the column. The steel tube wall is divided as triangular elements, which are treated as rigid body and connected by elastic springs. The elastic stiffness K_c of the column model is obtained by

$$K_c = \frac{16D_p}{x+a}\left(\frac{D_m}{\kappa^3 x^2}+\frac{\kappa}{x}+\frac{2}{\kappa x}+\frac{2\kappa}{D_m}\right) \quad (1)$$

Where, D_m is the distance between two plate thickness center of column flanges, D_p is the flexural rigidity of the plate per unit width, and a is the distance from the side of the beam flange to the plate thickness center of the column flange. x in Eq.(1) is obtained by a regression equation where calculated values of the elastic stiffness K are equal to experimental and numerical values in Ref.2, and κ, which determines the measure of height direction of the column model, is obtained by the condition of minimizing K. x and κ are given by

$$x = \alpha D_c (D_c/B_f)^{\beta} (D_c/t_c)^{\gamma} \quad (2.a)$$

$$\kappa = \sqrt{\frac{D_m\left\{1+\sqrt{7+(3D_m/x)}\right\}}{2x+D_m}} \quad (2.b)$$

Where D_c and t_c are respectively the outer diameter and thickness of the column, B_f is the width of the beam flange. Ref.2 has proposed $\alpha = 0.60$, $\beta = 0.50$, and $\gamma = -0.28$ for coefficients in Eq.(2.a). The elastic stiffness K is obtained by parallel connect of two models so that all displacements in the load direction at the point ○ of the exterior diaphragm model and the column model are matched. Therefore, K is given by

$$K = K_d + K_c \quad (3)$$

Next, in calculating the yield strength P_y, the following states 1 to 4 are assumed for cross sections s_1 to s_3 of the exterior diaphragm model in Fig.4 or elastic springs of the column model in Fig.5. P_y is obtained by calculating the force at the earliest time to reach state 1 to 4.

State 1: Full plastic state in consideration of the bending moment and shear force at the cross section s_1.
State 2: Full plastic state in consideration of the bending moment and shear force at the cross section s_2.
State 3: Full plastic state in consideration of the bending moment and axial force at the cross section s_3.
State 4: Bending moment of all elastic springs in the column model reaches the yield bending moment.

2.2 Beam-end connection

This chapter extends to entire beam-end connections including the beam web joint with the hollow column or CFT column. As shown in Fig.6, in the case of the exterior diaphragm type, the stress of the beam web joint is considered to be extremely low, considering out-of-plane deformation of the column. In this paper, the elastic stiffness K_j and the yield strength ${}_jM_y$ of the beam-end connection are calculated by ignoring the stress of beam web joints and considering only the stress of the beam flange joint. Assuming that the compression side of the joint bears the same magnitude of stress P as the tensile side, the bending moment ${}_jM$ of the beam-end connection is obtained by

$${}_jM = P \cdot d_b \quad (4)$$

Where, d_b is the distance between thickness centers of beam flange plates. Furthermore, it is assumed that the same magnitude of deformation δ occurs on the tensile side and on the compression side in case of the hollow column, on the other hand, in case of the CFT column, the same amount of deformation δ on the tensile side as on the hollow column occurs and the compression side is rigid. The rotation angle θ_j of beam-end connections is expressed by

Hollow column: $\theta_j = 2\delta/d_b$ (5.a)
CFT column: $\theta_j = \delta/d_b$ (5.b)

From Eq.(4) and (5), the elastic stiffness K_j in the ${}_jM$ - θ_j relationship can be obtained by

Hollow column: $K_j = K \cdot d_b^2/2$ (6.a)
CFT column: $K_j = K \cdot d_b^2$ (6.b)

The yield strength ${}_jM_y$ of the beam-end connection is calculated by replacing the load P in Eq.(4) with the yield strength P_y of the beam flange joint in case of both hollow columns and CFT columns. Therefore, ${}_jM_y$ is obtained by

$$ {}_jM_y = P_y \cdot d_b \tag{7}$$

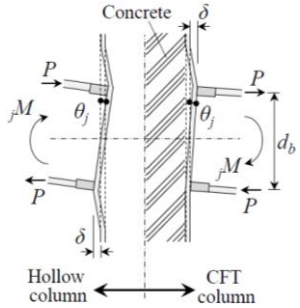

Fig.6 - Deformation of beam-to-column connection

3. FEA of beam flange joint using CFT column

3.1 Analysis overview

In this chapter, the validity of evaluation methods is confirmed by performing FEA using CFT columns and comparing calculated values based on Ref.2 with numerical values. The geometrically non-linear finite element analysis Abaqus ver. 6.12 is used for FEA. The schematic diagram of specimen is shown in Fig.7. The elements are 8-node hexahedral three-dimensional solid elements. Material properties are defined by the stress-strain relationship shown in Fig.8. The grade of columns is the 780N/mm^2 class steel H-SA700B, and the grades of beam-flanges and exterior diaphragms are the 550N/mm^2 class steel. The yield condition is based on yield condition of Mises, and the isotropic hardening rule is given. Concrete is treated as the elastic body, and Young's modulus E_c of concrete is 40000 N/mm^2. The contact condition between the inner surface of the column and concrete is rigid, and the friction coefficient is set to zero. Table1 shows the list of analysis cases. The analysis parameters are the column outer diameter D_c and thickness t_c, the beam flange width B_f and thickness t_b, and the exterior diaphragm depth h_d and thickness t_d. Note that the analysis outline shown in Table1 is the same as that of Ref.2 except that CFT columns is used. The same loads P are applied to the beam flange ends on both sides. The displacements in the loading direction at points T, S and C in Fig 7 are defined as respectively u_T, u_S and u_C, and the amounts of local deformation δ_T on the tensile sides and δ_C on the compression sides are defined as u_T - u_S and u_C - u_S, respectively. The validity of the FEA model using CFT column is confirmed by comparing load-deformation relationships of beam-end connections obtained by the experiment and FEA using cruciform frames as described later in the Section 4.2.

Table1 Summary of FEA

No.	Column (H-SA700B)		Beam flange (550N/mm^2 class)		Exterior diaphragm (550N/mm^2 class)	
	D_c (mm)	t_c /D_c	B_f /D_c	t_b /D_c	t_d /D_c	h_d /D_c
C36 – C58	700 – 1200	0.040 – 0.071	0.30 – 1.0	0.032 – 0.057	0.042 – 0.071	0.060 – 0.13

※ C55 and C56 are disused numbers.

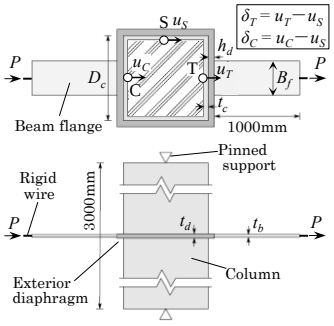

Fig.7 - Schematic diagram of specimen

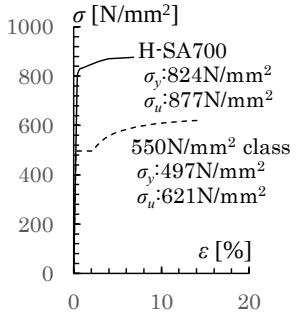

Fig.8 - Stress-strain relationship

3.2 Results of FEA

Fig.9 shows load-deformation relationships for each parameters, and C38 is the standard case. In Fig.9, the P - δ_C relationship of the CFT column is shown by black dashed lines, the P - δ_T relationship of the CFT column is shown by solid black lines, and the P - δ_T relationship of the hollow column is shown by gray solid lines. The point ● and ○ indicate the yield strength P_y of FEA in case of CFT columns and hollow column, respectively, and P_y is defined as the load P at the point when tangential stiffness decreases to 1/3 of the initial stiffness in P - δ_T relationship. From Fig.9, the elastic stiffness of the tensile side using CFT columns is slightly higher than that of hollow columns, and the yield strength is almost equal to that of hollow columns. Additionally, it can be seen that the deformation δ_C on the compression side of the CFT column is much lower than that on the tensile side.

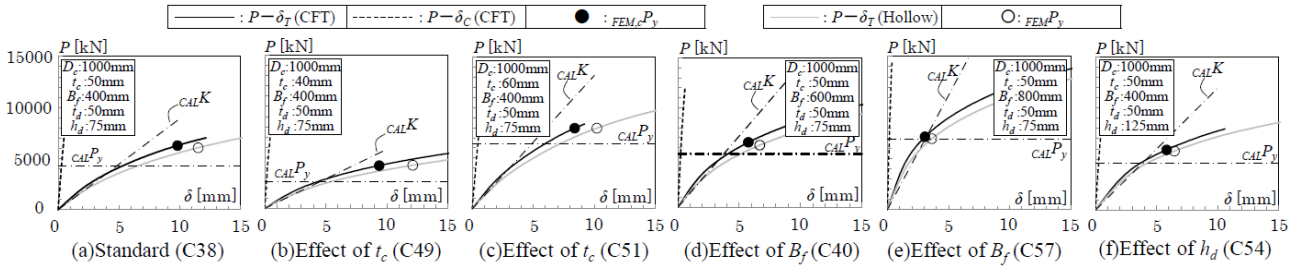

Fig.9 - Load-deformation relationship

Fig.10(a) shows the ratio of the elastic stiffness K between the CFT column and the hollow column on the tensile side, and Fig.10(b) shows the ratio of yield strength P_y between the CFT column and the hollow column on the tensile side. The horizontal axis shows the analysis number. Regarding the definitions of the symbols, ${}_{FEM}K$ and ${}_{FEM}P_y$ are respectively numerical values of the elastic stiffness and yield strength of the hollow column, ${}_{FEM,c}K_T$ and ${}_{FEM,c}P_y$ are respectively the numerical values of the elastic stiffness and yield strength of the CFT column on the tensile side. As shown in Fig.10(a), the elastic stiffness on the tensile side in case of CFT columns is increased by about 10 - 20% compared to that in case of hollow columns. This is due to the fact that the filled concrete restrains the bending and shear deformation in the side part of the exterior diaphragm on the tensile side. Furthermore, as shown in Fig.10(b), the yield strength of the CFT column is slightly higher than that of the hollow column, but the difference is less than 10% at the maximum. Fig.11 shows the elastic stiffness for each parameter. The point ○ indicates numerical values ${}_{FEM}K$ of the hollow column and ● indicates numerical values ${}_{FEM,c}K_T$ of the CFT column on the tensile side. In Fig.11(a) and (c), it can be seen that the elastic stiffness of the CFT column increases as the difference between the column outer diameter D_c and the beam flange width B_f becomes lower, similarly to that of the hollow column. Therefore, it is considered that the elastic stiffness of the joint can be increased by widening the beam flange with horizontal haunches. In Fig.11(a) - (d), the elastic stiffness in case of CFT columns is about 10 - 20% higher than that in case of hollow columns, and the rates of change of the elastic stiffness for each parameters are approximately the same for CFT columns and hollow columns.

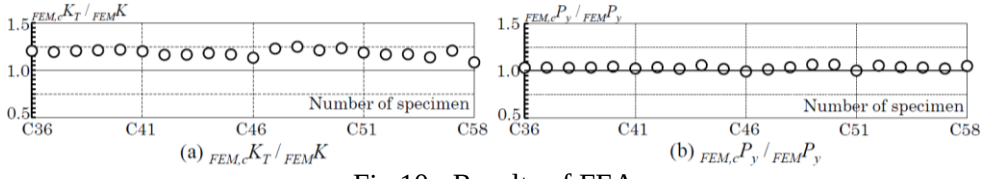

Fig.10 - Results of FEA

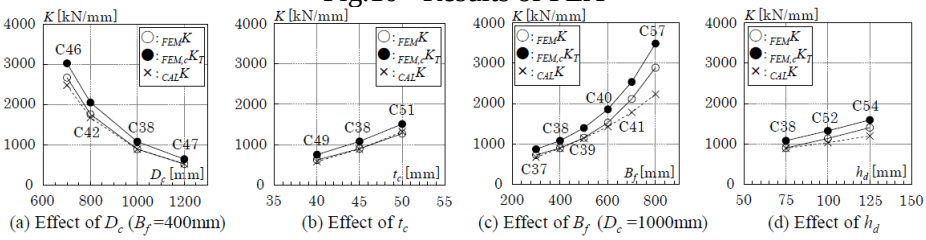

Fig.11- Effect of each parameters on elastic stiffness

3.3 Comparison between calculated values and numerical values

Fig.12 shows comparisons between calculated values and numerical values of the elastic stiffness and yield strength. Regarding the elastic stiffness on the tensile side using CFT columns in Fig.12(a), in most cases, calculated values are about 10 - 30% lower than numerical values. In the case C45 and C57, whose beam flange width B_f is large, the calculated value is 36% lower than the numerical value. As for the yield strength, in case of CFT columns, calculated values are at most 40% lower than numerical values as shown in Fig.12(b). In Fig.9, calculated values of the yield strength capture the point at which the stiffness begins to slightly decrease from the vicinity of the linear limit, and this evaluation method gives lower values than the strength at 1/3 tangential stiffness.

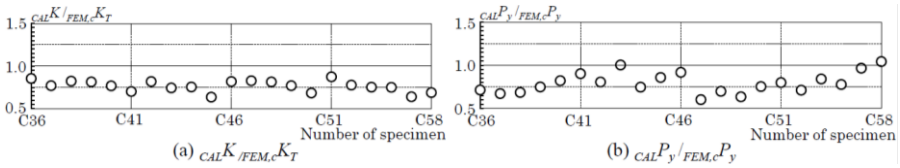

Fig.12 - Comparison of calculation and FEA

4. Cyclic loading test and FEA

Cyclic loading tests of cruciform frames are conducted shown in Fig.13 to confirm the elasto-plastic behaviors of entire beam-end connections including frames and beam webs until the frame reaches the final state. Even if the thickness of diaphragm is increased and the depth is reduced, it is confirmed that premature fracture does not occur at the exterior diaphragm and the beam. In addition, the validity of evaluation methods of the elastic stiffness and the yield strength of beam-end connections shown in section 2.2 is verified.

4.1 Outline of the experiment

Table2 shows the list of test specimens, Table3 shows mechanical properties of steel materials, and Table4 shows mechanical properties of filled concretes. The height of specimens is 1460mm and span l_s is 2250mm. The size of box-section columns using the 780N/mm^2 steel H-SA700B is □-200×12 with five hollow columns and three CFT columns. The beam is the H-section steel using SN490B (BH-300×B_b×12×19 or 300×90×6×16). The grade of exterior diaphragm is SN400B or SN490B. Fig.14 shows details of fillet welding between the column and the exterior diaphragm and welding materials are JIS Z 3312 YGW18. The experimental parameters are the depth h_d of the exterior diaphragm, the beam width B_b, the presence or absence of the horizontal haunch shown in Fig.15, and the hollow column or the CFT column. CF1 and CF5 are standard cases for respectively hollow columns and CFT columns, and beam flexural yielding preceding type specimens. CF2 and CF6 with small h_d are specimens of exterior diaphragm yielding preceding type. CF3 is the specimen that changes the beam width B_b and precedes shear yielding at the front of the exterior diaphragm. CF4 and CF7 are test specimens whose beam-ends are widened with the horizontal haunch. CF8 has the hollow column, and the difference in mechanical behaviors of beam-end connections between the CFT column and the hollow column is confirmed by comparing with CF5. While the out-of-plane deformation of beams is restrained by stiffening jigs, a shear force Q is applied to the top of the column by a hydraulic jack. Both ends of the beam are connected by link members, and the lower end of the column is supported by the pin. Fig.16 shows the loading protocol. The loading protocol is cyclic loading of positive and negative alternations, the inter-story deformation angle R is increased by 0.01rad, and the loading is repeated twice at the same inter-story deformation angle.

CF1, CF4, CF5, CF7 and CF8 are beam yielding preceding type specimens, and their design method is shown below. Considering the bending moment diagram of the beam shown in Fig.18, when the beam at the horizontal haunch start position reaches the plastic moment $_bM_p$, it is assumed that the bending moment $_jM_{bp}$ acts on the beam-end connection. The beam yielding preceding type specimens are designed so that the yield strength $_jM_y$ of connections is equal to or higher than $_jM_{bp}$. That is, the following equation is satisfied.

$$_jM_y / {}_jM_{bp} \geqq 1 \qquad (8)$$

Table 2 shows the strength ratio ${}_jM_y/{}_jM_{bp}$. In CF1, CF4, CF5, CF7 and CF8, ${}_jM_y/{}_jM_{bp}$ exceeds 1.0. In CF2 and CF6 where ${}_jM_y/{}_jM_{bp}$ is lower than those of other specimens, it is assumed that the beam-end connection yielding precedes the beam. Because it is possible that the strength of the connection panel may be reduced due to the influence of out-plane deformation of columns, doubler plates are welded on the panel surface to reinforce the panels. The grade of doubler plates is H-SA700B with the same plate thickness (12mm) as the column.

Table2 Summary of cruciform frame specimen

No.	Column (H-SA700B)			Beam (SN490B)				Horizontal haunch		Exterior diaphragm			Doubler plate (H-SA700B)		${}_jM_y/{}_jM_{bp}$	Elastic stiffness			Yield strength		
	CFT	D_c (mm)	t_c (mm)	D_b (mm)	B_b (mm)	${}_bt_w$ (mm)	${}_bt_f$ (mm)	b_h (mm)	l_h (mm)	Grade	t_d (mm)	h_d (mm)	D_{dp} (mm)	t_{dp} (mm)		${}^{FEM}K_j$ ($\times 10^3$) (kN·m/rad)	${}^{CAL}K_j$ ($\times 10^3$) (kN·m/rad)	${}^{CAL}K_j/{}^{FEM}K_j$	${}^{FEM}{}_jM_y$ (kN·m)	${}^{CAL}{}_jM_y$ (kN·m)	${}^{CAL}{}_jM_y/{}^{FEM}{}_jM_y$
CF1	—	200	12	300	100	12	19	—	—	SN490B	40	70	155	12	1.11	133	109	0.82	353	295	0.84
CF2										SN400B		40			0.48	76.6	57	0.74	205	123	0.60
CF3					150					SN490B		70			0.96	164	154	0.94	388	342	0.88
CF4					100			55	125						1.32	190	211	1.11	411	402	0.98
CF5	○				90	6	16	—	—		32	65	125		1.06	163	152	0.93	280	209	0.75
CF6												40			0.67	107	87	0.81	233	128	0.55
CF7								55	100			65			1.39	247	331	1.34	-	306	-
CF8	—							—	—						1.06	107	76	0.71	265	209	0.79

D_b, B_b: Depth and width of beam, ${}_bt_w$, ${}_bt_f$: Thickness of beam web and flange, b_h, l_h: Width and length of haunch (see Fig.15), D_{dp}, t_{dp}: Width and thickness of doubler plate, ${}_jM_y$: Yield moment of beam-end connection (calculation), ${}_jM_{bp}$: Bending moment of beam-end connection which is acted when beam reaches full plastic state (calculation).

Table3 Mechanical property of steel

Grade	Applied part		t mm	σ_y N/mm²	σ_u N/mm²	ε_u %
H-SA700B	Column	CF1-4	12.0	816	856	26
		CF5-8	11.8	822	859	24
SN490B	Beam flange	CF1-4	18.9	326	522	44
		CF5-8	15.9	352	533	42
	Beam web	CF1-4	12.0	361	536	36
		CF5-8	6.78	343	491	41
	Exterior diaphragm	CF1,3,4	40.6	337	524	27
		CF5-8	32.0	332	524	31
SN400B		CF2	40.2	251	425	34

t : Thickness, σ_y: Yield stress, σ_u: Tensile stress, ε_u: Breaking elongation.

Table4 Mechanical property of filled concrete

Part	E_c N/mm²	f_c N/mm²	f_t N/mm²
CF5	3.98×10^4	70.0	3.93
CF6	4.00×10^4	73.4	4.23
CF7	3.70×10^4	67.8	3.31

E_c : Young's modulus of concrete,
f_c : Compressive stress, f_t : Tensile stress.

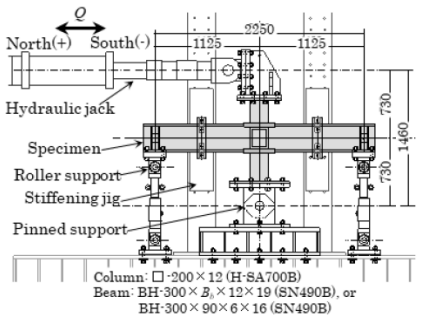

Fig.13 - Test setup (Unit: mm)

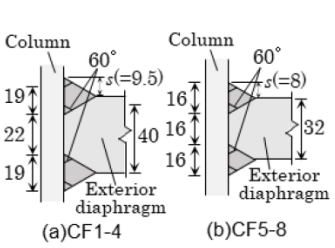

Fig.14 - Detail of welding (unit: mm)

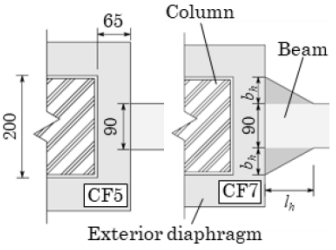

Fig.15 - Beam flange joints (unit: mm)

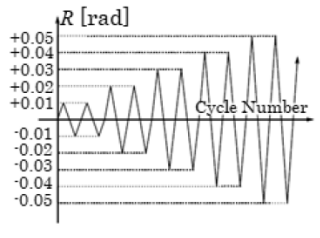

Fig.16 - Loading protocol

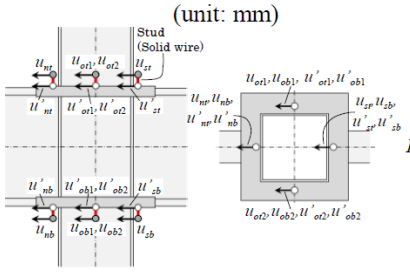

Fig.17 - Measurement method

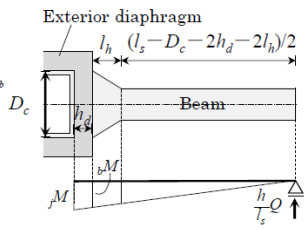

Fig.18 – Bending moment diagram

4.2 Analysis Overview

Performing FEA to simulate the experiment, it is confirmed that the load-deformation relationships of the beam-end connections obtained by the experiment and FEA is consistent, and the validity of the cruciform

frame model in this chapter is verified. Additionally, the effect of the difference in the output points for measuring the amount of local deformation indicated by ● or ○ in Fig.17 on the elastic stiffness of connections is confirmed by FEA.

Abaqus ver.2016 is used for FEA. Fig.19 shows the schematic diagram of the FEA model of CF1. The elements are 8-node hexahedral three-dimensional solid elements. The materials property of steels and filled concretes are defined by table3 and table4, respectively. The yield condition of Mises and the combined hardening rule combining the kinematic hardening rule and the isotropic hardening rule are given. The welding parts between the column and the exterior diaphragm is modeled with the same shape as in Fig.15, and the material property is defined by the tensile test result of the welding parts with YGW18. The concretes of CF5 - CF7 are modeled as the elastic body, and the material test results shown in Table 4 are used for Young's modulus. As in Chapter 3, contact condition between the inner surface of the column and the concrete is rigid, and the friction coefficient is zero. Regarding output points for measuring the local deformation of beam-end connections, output points ● are set at tips of rigid-bars on exterior diaphragms surface with the intention of simulating the experiment (Case A), and output points ○ are provided on the exterior diaphragm surface shown in Fig.17 (case B).

Fig.20 shows the relationship between the bending moment ${}_jM$ acting on the beam-end connection and the beam-end rotation angle θ_j obtained from experiments and FEA of Case A for CF1, CF5, CF6 and CF8. The black line indicates the experiment, the gray line indicates FEA of Case A, the solid line indicates the south side, and the dashed line indicates the north side of beam-end connections. In Fig.20, the ${}_jM$ - θ_j relationship between the experiment and FEA of Case A is almost the same, and it is confirmed that the experiment and FEA are in good correspondence, and FEA can simulate the experiment. Based on these results, the FEA model using CFT columns shown in the chapter 3 is considered to be generally valid. Next, Table5 compares the elastic stiffness ${}_{EXP}K_j$, ${}_{FEM,A}K_j$, ${}_{FEM,B}K_j$ of beam-end connections obtained from the experiment, FEA of Case A and FEA of Case B, respectively. The elastic stiffness ${}_{FEM,A}K_j$ based on FEA of Case A is 7 - 51% lower than the elastic stiffness ${}_{FEM,B}K_j$ based on FEA of Case B. This is because the exterior diaphragm is deformed by the beam-end bending moment and rigid bars on the exterior diaphragm surface are tilted, it is considered that the measurement of the local deformation of the beam-end connections includes errors in FEA of case A and the experiment. Therefore, after Section 4.3, the ultimate states and the load-deformation relationships of frames and beams are examined based on the experimental results, and the load-deformation relationship, the elastic stiffness and the yield strength of beam-end connections are examined based on the numerical results of Case B.

Table5 Summary of elastic stiffness K_j of experiment and FEA

No.	${}_{EXP}K_j$ ($\times 10^3$) (kN·m/rad)	${}_{FEM,A}K_j$ ($\times 10^3$) (kN·m/rad)	${}_{FEM,B}K_j$ ($\times 10^3$) (kN·m/rad)	${}_{FEM,A}K_j$ / ${}_{EXP}K_j$	${}_{FEM,A}K_j$ / ${}_{FEM,B}K_j$
CF1	87.1	73.2	133	0.84	0.55
CF2	58.9	47.4	76.6	0.80	0.62
CF3	102	83.7	164	0.82	0.51
CF4	112	92.3	190	0.82	0.49
CF5	156	150	163	0.96	0.92
CF6	99.4	100	107	1.01	0.93
CF7	208	226	247	1.09	0.91
CF8	111	96.3	107	0.87	0.90

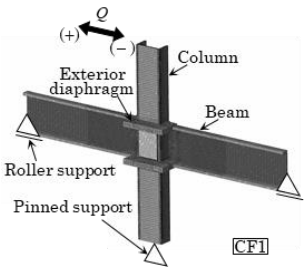

Fig.19 - FEA model

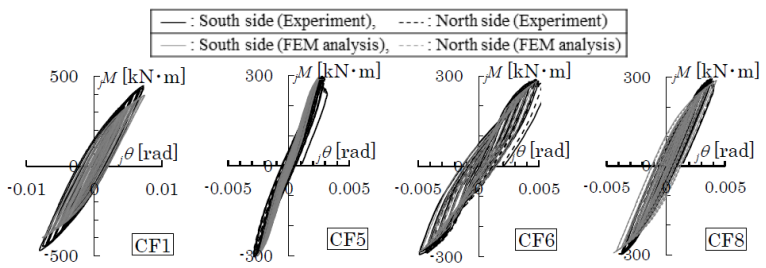

Fig.20 - ${}_jM$ - θ_j relationship of experiment and FEA

4.3 Experiment and numerical results

(1) Load deformation relationship and final state

The final states of the test specimens CF1 - CF8 in this experiment are classified into the following four types.

Final state 1: Fracture at the recessed corner of the exterior diaphragm shown in Fig.21(a).
Final state 2: Remarkable lateral buckling and local buckling of the beam shown in Fig.21(b).
Final state 3: Fracture at the toe of horizontal haunch shown in Fig.21(c).
Final state 4: Fracture of fillet welding parts between the column and the end plate at top of column.

CF2 with the lowest strength ratio ${}_jM_y$ / ${}_jM_{bp}$ is confirmed the final state 1. CF5 and CF6 using the CFT column, and CF8 using the hollow column are confirmed to be in the final state 2. CF7 using the CFT column with the horizontal haunch at the beam-end is confirmed to be in the final state 3. CF1, CF3, and CF4 using the hollow columns become the final state 4.

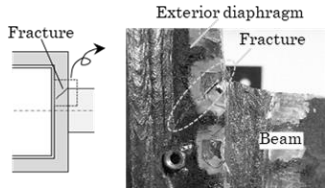

(a)Fracture of diaphragm (CF2)

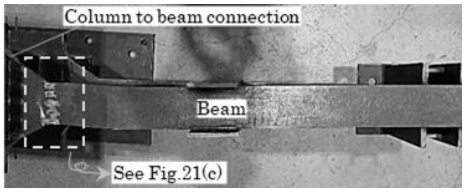

(b)Buckling of beam

(c)Fracture at toe of haunch

Fig.21 - Final states of specimens

Fig.22 shows relationships between the shear force Q and inter-story deformation angle R of CF2, CF8, CF7 and CF1 for the final states 1 - 4, respectively. In Fig.22, the horizontal load ${}_bQ_p$ when the beam reaches the plastic moment and the load ${}_jQ_y$ when the beam-end connection reaches the yield strength ${}_jM_y$ are shown. In the final states 1 - 3, Q - R relationships is almost the same, early fractures do not occur in the exterior diaphragms and beams, and sufficient plastic deformation capacity can be confirmed. In the final state 4, the history before fracture of the fillet welding is the same as those of other specimens, however, premature fracture occurs due to the insufficient welding size between the column and the end plate at top of the column. It is assumed that the plastic deformation capacity more than results of this experiment can be obtained by designing the sufficient welding size. Figs.23 shows the relationships between the bending moment ${}_bM$ acting on the beam and the beam deformation angle θ_b, and the relationships between the bending moment ${}_jM$ acting on the beam-end connection and the beam-end rotation angle θ_j for CF2 (final state 1), CF8 (final state 2) and CF7 (final state 3), respectively. The solid line represents the southern beam or beam-end connection, and the dashed line represents the northern beam or beam-end connections. In CF8 using the hollow column shown in Fig.23(b) and CF7 using the CFT column shown in Fig.23(c), the beam-end connection shows almost elastic behavior, and plastic deformation of the beam occurs mainly. On the other hand, in CF2, whose diaphragm depth h_d is short shown in Fig.23(a), plastic deformation of the beam-end connection occurs remarkably. In the cruciform frame using the exterior diaphragm proposed in this study, the column is made of 780N/mm^2 steel, which assumes the use of an elastic range, and it is necessary to keep the beam-end connection elastic in the final state. Therefore, the final state 2 or 3 are desirable, where the beam-end connections behave almost in the elastic manner and plastic deformation of the beam occurs mainly.

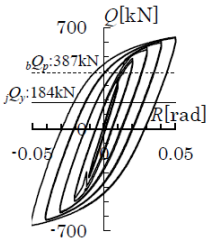

(a)CF2

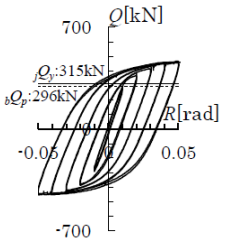

(b)CF8

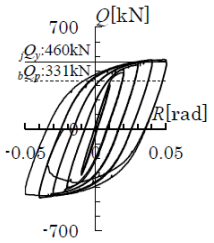

(c)CF7

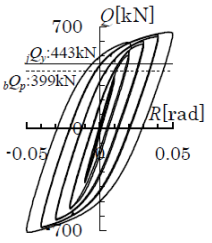

(d)CF1

Fig.22 - Q - R relationship (Experiment)

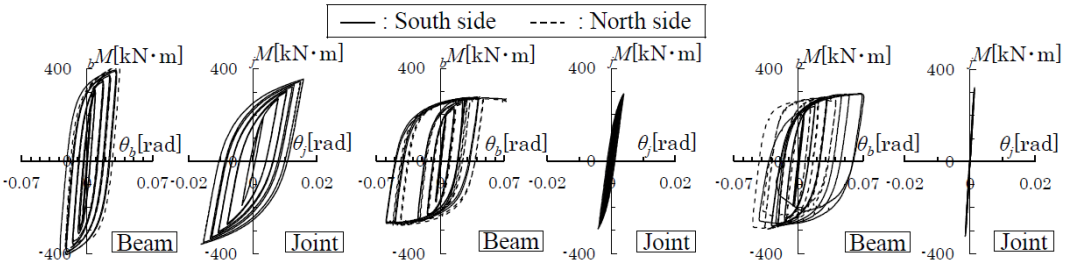

(a)CF2(final state 1) (b)CF8(final state 2) (c)CF7(final state 3)

Fig.23 - ${}_bM$ - θ_b relationship (Experiment) and ${}_jM$ - θ_j relationship (FEA)

(2) Elastic stiffness and yield strength of beam-end connection

Table2 shows the elastic stiffness ${}_{FEM}K_j$ and yield strength ${}_{FEM,j}M_y$ of the beam-end connection obtained from the analysis of Case B. The yield strength ${}_{FEM,j}M_y$ is the bending moment when the tangential stiffness is reduced to 1/3 of the initial stiffness in the ${}_jM$ - θ_j relationship. In addition, the numerical value of CF7 is not shown because the tangential stiffness do not decrease to 1/3 of the initial stiffness. Fig.24 shows numerical values of the elastic stiffness and yield strength for each parameters. The values ${}_{FEM(1)}K_j$, ${}_{FEM(5)}K_j$ and ${}_{FEM(8)}K_j$ represent the analysis values of the elastic stiffness of CF1, CF5 and CF8, respectively, and ${}_{FEM(1),j}M_y$, ${}_{FEM(5),j}M_y$, ${}_{FEM(8),j}M_y$ indicate the numerical values of the yield strength of CF1, CF5 and CF8, respectively. The numerical values of CF1, CF5 and CF8 are divided by results of each specimens on the vertical axis.

Regarding the elastic stiffness, as shown in Fig.24(a), the elastic stiffness of CF2 and CF6 having short h_d are about 40% lower than that of the standard specimen CF1 and CF5, respectively. According to Fig.24(b), the elastic stiffness of CF4 and CF7 with horizontal haunches increases by about 50% than that of CF1 and CF5, respectively. Furthermore, as shown in Fig.24(c), because the filled concrete inside the column restrains the bending and shear deformation of the tensile side and the compression side of the beam-end connection, the elastic stiffness of CF5 with the CFT column is 50% higher than that of CF8.

Next, regarding the yield strength, as shown in Fig.25(a), CF2 and CF6 are about 20 - 40% lower than that of CF1 and CF5, respectively. As shown in Fig.25(b), the yield strength of CF4 is 10 - 20% higher than that of CF1. Furthermore, from Fig.25(c), yield strength of CF5 using CFT columns is less than 10% different from that of CF8 using hollow columns.

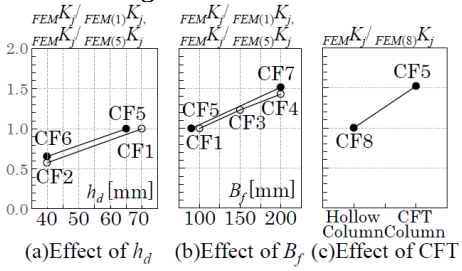

(a)Effect of h_d (b)Effect of B_f (c)Effect of CFT

Fig.24 - Numerical results of elastic stiffness

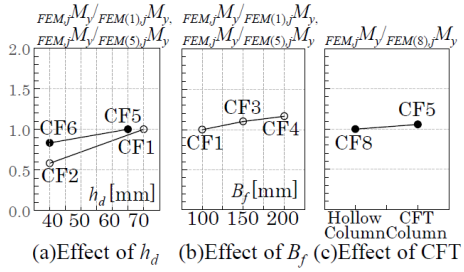

(a)Effect of h_d (b)Effect of B_f (c)Effect of CFT

Fig.25 - Numerical results of yield strength

(3) Comparison between numerical values and calculated values of elastic stiffness and yield strength

Table2 compares calculated values ${}_{CAL}K_j$, ${}_{CAL,j}M_y$ with numerical values of Case B of the elastic stiffness and yield strength of beam-end connections. The elastic stiffness of CF4 and CF7 with the horizontal haunch is about 11 - 34% larger than the numerical value. This is because the accuracy of the evaluation method is greatly affected by the beam width B_f, and the ratio of calculated values to numerical values tends to increase as the beam width B_f increases. However, for other specimens, calculated values are slightly lower than numerical values, and the difference is evaluated within 7 - 29%. On the other hand, with respect to the yield strength, calculated values are 40 - 45% lower than the numerical values of CF2 and CF6 where the depth h_d of the exterior diaphragm is short. This factor is described below. In the analysis, the shape and material properties of the fillet welds between the column and the exterior diaphragm shown in Fig.14 are considered to simulate the experiment, but in the calculation of elastic stiffness and yield strength, the fillet welds is ignored. It is conceivable that the fillet welds bear higher stress than the base metal when the beam-end

connection yields, and the yield strength of the beam-end connections increases. In particular, in the case where the depth h_d of the exterior diaphragm is small, the ratio of fillet welds in the cross section shown in Fig.14 is higher than in the other specimens, and the difference between the numerical value and the calculated value may be larger. However, for other test specimens, the calculated yield strength is evaluated by a difference within 25% of numerical values.

5. Conclusion

In this study, for the 780N/mm^2 class steel box-section CFT column to beam-flange joint with the exterior diaphragm, which is reduced depth and increased thickness instead, calculated values of the elastic stiffness and the yield strength are compared with the results of FEA using local models to verify the validity of the evaluation methods proposed in Ref.2 and 3, and the following findings are obtained.

[1] In case of the CFT column, the local deformation of the side part of the exterior diaphragm is restrained by the filled concrete, and numerical values of the elastic stiffness of the beam-flange joints on the tensile side increases by about 10 - 20% compared to those in case of the hollow column. In addition, at the compression side of beam-flange joints, the local deformation is significantly suppressed by the filled concrete.

[2] Numerical values of the yield strength of the beam-flange joints are almost the same in case of hollow columns and CFT columns.

[3] Most calculated values are about 10 - 30% lower than numerical values, and both calculated values and numerical values show good correspondence with any parameters. In addition, calculated values of the yield strength can capture the vicinity of the linear limit strength of the beam-flange joints even in case of CFT columns.

The elasto-plastic behaviors of the beam-end connections are confirmed by cyclic loading tests and FEA of cruciform frames. The following findings are obtained by comparing the calculated values based on the evaluation methods proposed in Chapter 2 with results of experiments and FEA.

[4] It is confirmed that calculated values of both the elastic stiffness and the yield strength can be evaluated with the difference between the numerical values within about 10 - 30% in most specimens.

[5] In the high strength steel column to beam connections proposed in this study, it is desirable that the beam-end connections including the steel tube wall keep elastic behavior in the final state of the frame. Adapting the proposed evaluation methods to design the beam-end connection, even if the depth of exterior diaphragm is reduced instead of increasing the plate thickness, premature fracture do not occur at the diaphragm and the beam, and it is confirmed that the beam-end connections show almost elastic behavior in specimens, on which yield strength of beam-end connections is equal to or higher than full plastic moment of beams, in the final state.

6. References

[1] The Japan iron and Steel Federation: Standard and Summary of Welding Construction of 780N/mm^2 Class High Strength Steel (H-SA700) for Building Structures, 2012.11

[2] Oba, R., Kinoshita, T., Suita, K., Koetaka, Y., Matsuo, S., and Murakami, Y.: Evaluation of Elastic Stiffness and Yield Strength of High Strength Steel Box-Shaped Column to Beam Flange Joint in an Exterior Diaphragm Moment Connection, Journal of Structural and Construction Engineering (Transactions of AIJ),Vol.81 No.730, pp.2123-2132, 2016.12

[3] Oba, R., Kinoshita, T., Suita, K., Koetaka, Y., Matsuo, S., and Murakami, Y.: Evaluation of Elastic Stiffness and Yield Strength of High Strength Steel Square Tube Column to Beam Flange Connections with Exterior Diaphragm, 16th World Conf. on Earthquake Engineering, Paper No.808, 2017.1

[4] Kawai, T. and Kondou, K.: Collapse Load Analysis of Bending Plates by a New Discrete Model, Journal of The Society of Naval Architects of Japan, No.142, pp.190-196, 1977.12

